Applied Surface Science 335 (2015) 44–49

Contents lists available at ScienceDirect

Applied Surface Science

journal homepage: www.elsevier.com/locate/apsusc

In situ stress measurements during pulsed laser deposition of $BaTiO_3$ and $SrTiO_3$ atomic layers on Pt(0 0 1)

J. Premper*, D. Sander, J. Kirschner

Max-Planck-Institut für Mikrostrukturphysik, Weinberg 2, D-06120 Halle/Saale, Germany

ARTICLE INFO

Article history:
Received 17 December 2014
Received in revised form 30 January 2015
Accepted 1 February 2015
Available online 9 February 2015

Keywords:
Cantilever stress measurements
Film stress
PLD
$BaTiO_3$
$SrTiO_3$
Thin films

ABSTRACT

We apply the cantilever deflection technique to measure stress in nm thin $BaTiO_3$ and $SrTiO_3$ films during pulsed laser deposition on a Pt(0 0 1) single crystal cantilever substrate. We find a compressive film stress of −4.2 GPa for $BaTiO_3$ on Pt(0 0 1) (misfit = −2.3%), whereas the deposition of $SrTiO_3$ (misfit = +0.4%) induces a tensile stress of +1.5 GPa. The stress measurements are augmented by *in situ* low energy electron diffraction experiments which indicate an epitaxial order of the films. We apply continuum elasticity to calculate film stress. We conclude that sign and magnitude of the measured stress are due to the epitaxial misfit between film and substrate, which is −2.3% and +0.4% for $BaTiO_3$ and $SrTiO_3$, respectively.

We identify that in addition to misfit also the oxygen partial pressure during PLD film growth influences film stress. PLD growth in an oxygen-free environment leads to factor of two increased tensile stress in $SrTiO_3$ on Pt(0 0 1) as compared to growth at $p_{O_2} = 10^{-4}$ mbar. The role of film stoichiometry for film stress is discussed.

© 2015 Elsevier B.V. All rights reserved.

1. Introduction

Thin films of perovskite oxides attract considerable attention in the field of superconductivity [1], and for photovoltaic [2], storage and micro-structured electronic devices [3–6]. This is also due to their intriguing coupling between mechanical, structural and electronic properties [7].

Structure studies of bulk $BaTiO_3$ and $SrTiO_3$ started some 70 years ago [8–10], and thin film growth by pulsed laser deposition (PLD) was realized more than 20 years ago [11–13]. In spite of this long tradition of the study of these prototypical perovskite materials, many fundamental question are still open, especially for thin films in the nm thickness range. Recent investigations focus, *e.g.* on their structural [14–17] and electronic properties [18–20].

Current interest is spurred also by the coupling between strain and stress in perovskite oxide films, which is pivotal for their multiferroic properties [21]. For these applications a characterization of the mechanical properties of nm thin perovskite films is mandatory. One issue in this respect is whether atomic layers of just a few unit cell thickness show the same elastic behavior as their bulk counterparts. Stress measurements [22] have established a quantitative understanding of stress–strain relations in molecular beam epitaxial growth of metallic atomic layers [23–27], in sputtered films [28] and in PLD grown metallic atomic layers [29,30]. These previous studies indicate that nm thin metallic films can be reliably characterized by their bulk elastic properties. Corresponding measurements for oxide films are scarce [31].

In this study we extend the application of the cantilever curvature stress measurements to PLD growth of the prototypical perovskite oxides $BaTiO_3$ and $SrTiO_3$ on Pt(0 0 1) [14,16]. This application of the stress measurement is experimentally challenging, as it involves stress measurements at a high sample temperature of order 900 K, in a substantial oxygen partial pressure of order 10^{-4} mbar. The high temperature and the appreciable oxygen partial pressure deviate sharply from the typical UHV growth conditions of metal films of previous stress studies, but nevertheless reliable quantitative stress data were obtained and are presented here.

We combine stress measurements by the crystal curvature technique with medium energy electron diffraction (MEED) intensity measurements during film growth. This allows to characterize the growth behavior and to monitor the film thickness with high precision [26,32]. The epitaxial order of the films is examined by *in situ* low energy electron diffraction (LEED).

In this work we answer the following as-of-yet open questions: (i) What is the magnitude of film stress in epitaxial $BaTiO_3$ and $SrTiO_3$ films? (ii) Does continuum elasticity apply to $BaTiO_3$ and $SrTiO_3$ single layers? (iii) What is the proper reference state for the

* Corresponding author. Tel.: +49 3455582745.
E-mail address: jpremper@mpi-halle.de (J. Premper).

http://dx.doi.org/10.1016/j.apsusc.2015.02.009
0169-4332/© 2015 Elsevier B.V. All rights reserved.

structure of $BaTiO_3$? This question is highly relevant, as $BaTiO_3$, in contrast to $SrTiO_3$, exhibit a structural phase transition as bulk material from a tetragonal to a cubic phase at the temperature of film growth. (iv) How does the oxygen partial pressure during PLD influence film stress?

We find that epitaxial growth of these perovskite films induces considerable stress of several GPa, where sign and magnitude of the stress indicate epitaxial misfit as a dominant factor for the resulting stress magnitude.

2. Stress and PLD experiment

We combined an optical stress-induced crystal curvature measurement [25,36–38] with a PLD experiment. Sample preparation, film growth and stress measurements are performed in the same UHV chamber. Thin single crystal substrates (thickness t_S = 0.1 mm) are used for our stress measurements [39]. They have lateral dimensions of 12 mm × 2.5 mm. The sample has a large length-to-width ratio of 4, which minimizes clamping effects on the stress-induced curvature, and this ensures accurate stress measurements [25,40,41].

Crystal curvature stress measurement require fairly thin (≈0.1 mm) substrates. We tried $SrTiO_3$ and $BaTiO_3$ substrates, but the brittle nature of these materials was incompatible with the cantilever clamping and heating process of the curvature measurement, and the substrates broke repeatedly. Thus, we revert to metal single crystals, which do not suffer from these limitations. We use Pt single crystals as substrates. The lattice constant (3.920 Å) allows us to probe the effect of positive and negative misfit on the resulting stress for the film materials $SrTiO_3$ and $BaTiO_3$, respectively. The Pt(0 0 1) crystal was cleaned by sputtering with Ar^+ ions (beam energy 1.5 keV, sample current 1 μA, 30 min), annealed in oxygen ($p_{O_2} = 5 \times 10^{-7}$ mbar at 800 K for 30 s) and heated to 1300 K for 5 s.

Low energy electron diffraction (LEED) measurements show in Figs. 1(b) and 2(b) the diffraction pattern of the clean Pt(0 0 1) surface with its well known Pt(0 0 1)-hex reconstruction [42]. Auger electron spectroscopy reveals a clean surface, where the contamination level is below 1% surface coverage.

$BaTiO_3$ and $SrTiO_3$ films were grown by PLD from stoichiometric targets [43,44] on Pt(0 0 1). We used an KrF excimer laser [45] with a wavelength of 248 nm, pulse energies of 120–150 mJ and a frequency of 2 Hz. The laser fluence at the target surface was in the range of 2.0–2.7 J/cm^2. The PLD target and the Pt(0 0 1) substrate are aligned at an angle of 39°. We use a computer-controlled mirror to scan the PLD laser beam across the stationary target.

The film thickness was monitored *in situ* by MEED intensity oscillations and independently by a quartz microbalance [46]. This gives a film thickness accuracy of ± 0.2 ML. The film thickness is given in unit cells (uc), where one uc corresponds to the $BaTiO_3$ or $SrTiO_3$ lattice constant, respectively, *i.e.* 1 uc_{BaTiO_3} = 0.4012 nm and 1 uc_{SrTiO_3} = 0.3905 nm [47].

PLD of $BaTiO_3$ and $SrTiO_3$ is performed at substrate temperatures of 900 K at an oxygen partial pressure of $p_{O_2} = 1 \times 10^{-4}$ mbar. Similar preparation conditions were reported in literatures [48–50]. Deposition temperature and oxygen partial pressure have been optimized to give the sharpest LEED diffraction spots.

Note that the experimental conditions to prepare epitaxial $BaTiO_3$ and $SrTiO_3$ films are challenging for stress and MEED measurements. High substrate temperatures of 900 K require large heating powers of 100 W, which unavoidably lead to thermal drift and light emission. The first is detrimental for stress measurements, the latter for MEED intensity measurements. An elaborated filament shielding was successfully implemented to ensure reliable stress measurements at these conditions.

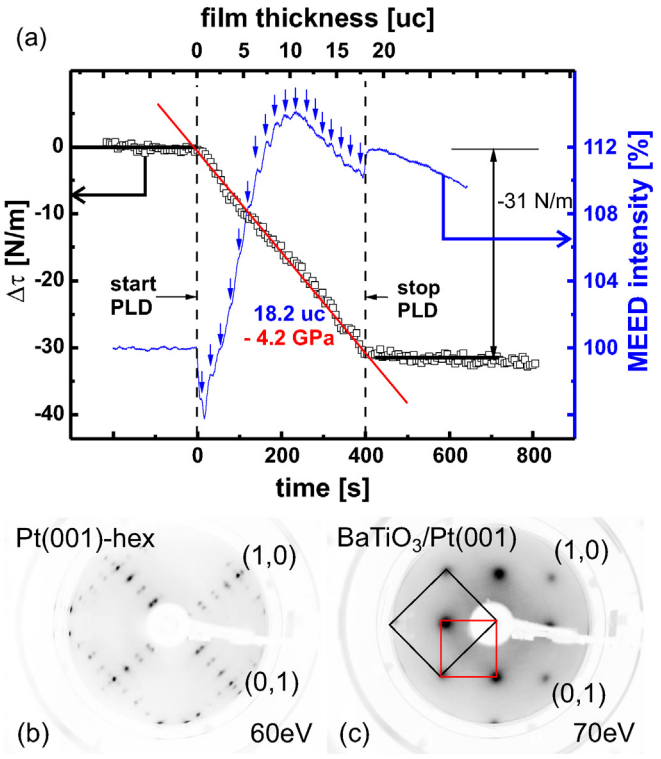

Fig. 1. Stress change $\Delta\tau$ (black squares) and MEED intensities (blue line) during PLD growth of $BaTiO_3$ on Pt(0 0 1). Vertical lines indicate when the PLD deposition started and stopped (T_{growth} = 900 K, $p_{O_2} = 1 \times 10^{-4}$ mbar). The LEED diffraction image below the stress measurement shows the clean substrate surfaces before PLD growth (b). Additional diffraction spots along [0,1] and [1,0] indicate the so-called hexagonal reconstruction of Pt(0 0 1) [42]. The diffraction pattern after growth (c) shows a c(2 × 2) superstructure (red square), where the 1 × 1 mesh is indicated in black. (For interpretation of the references to color in this figure legend, the reader is referred to the web version of the article.)

We extract film stress from the stress-induced curvature change of the substrate. After reaching thermal equilibrium at the substrate temperature of 900 K within 1 h of sample preparation, film stress was measured [25,36–38] during PLD of $BaTiO_3$ and $SrTiO_3$. Eq. (1) is applied [25,40,41] to obtain the stress change $\Delta\tau_S$ from the curvature change $\Delta\kappa = \Delta(1/R)$:

$$\Delta\tau_S = \Delta(\tau \cdot t_f) = \frac{Yt_S^2}{6(1-\nu)}\Delta\kappa, \quad (1)$$

where the Young modulus Y and the Poisson ratio ν are calculated for the specific surface orientation of the sample [51]. Table 1 gives the respective values. The film stress τ is derived from the slope (red line in Figs. 1–3) of the stress curves as a function of film thickness.

A benefit of the 2-beam curvature measurements over a single beam deflection measurement is the improved noise reduction by subtracting both position signals from each other, and this makes the stress measurements also more robust against thermal drift. Reliable results are obtained with a very high sensitivity even during growth at 900 K. A more detailed description of the technique can be found in [25,36,38,52,53].

3. Results

In the following we present results on $BaTiO_3$- and $SrTiO_3$-induced film stress on Pt(0 0 1) in Figs. 1(a) and 2(a). $BaTiO_3$ and $SrTiO_3$ are chosen as film materials in order to clarify the role of misfit, which is positive and negative with respect to

Table 1
Elastic compliance constants s_{ij}, Young modulus Y, Poisson ratio ν and biaxial modulus $Y/(1-\nu)$ for substrate and film. Y and ν are given for the [1 0 0]-direction, since they are anisotropic within the (0 0 1)-plane. The biaxial modulus $Y/(1-\nu)$ is isotropic in the (0 0 1)-plane.

Substrate or film	s_{11} (TPa^{-1})	s_{12} (TPa^{-1})	s_{13} (TPa^{-1})	s_{33} (TPa^{-1})	s_{44} (TPa^{-1})	s_{66} (TPa^{-1})	Y (GPa)	ν	$\frac{Y}{1-\nu}$ (GPa)	Reference
Pt(0 0 1)	7.35	−3.08			13.1		136	0.42	234	[33]
$BaTiO_3(0\,0\,1)_{cub}$	8.7	−3.35			8.9		115	0.39	187	[34]
$BaTiO_3(0\,0\,1)_{tetr}$	7.35	−1.39	−4.94	14.95	18.21	8.33	136	0.19	168	[35]
$SrTiO_3(0\,0\,1)_{cub}$	3.75	−0.92			8.15		267	0.25	353	[34]

Pt(0 0 1), respectively. We also present stress measurements for $SrTiO_3$/Pt(0 0 1) grown under different oxygen partial pressures in Fig. 3(a) to elucidate the partial pressure influence on film stress.

All the figures are organized in the same way. Stress changes are plotted as black data points. The blue lines show the simultaneously obtained MEED intensity, where small blue arrows are a guide for the eye to identify periodic changes, which are related to increments of the film thickness by one uc. This interpretation is supported by independent thickness measurements by a quartz microbalance. Quartz microbalance data were used for the thickness calibration in cases where only small MEED oscillations could be obtained.

Fig. 1(a) shows a monotonic negative stress change upon $BaTiO_3$ growth on Pt(0 0 1). The slope of the stress curve indicates a compressive film stress of −4.2 GPa. In contrast, Fig. 2(a) for $SrTiO_3$/Pt(0 0 1) shows a tensile stress change, where the slope gives a film stress of +1.5 GPa. The LEED images indicate pseudomorphic growth for both films. The white and the red squares show the fcc Pt lattice unit cell and a c(2 × 2) superstructure of the film, respectively. This epitaxial order was also found in previous works [15,17].

We examined also the influence of the oxygen partial pressure on film stress, as shown in Fig. 3. In comparison to the stress curve of Fig. 2(a) with a film stress of +1.5 GPa, we find a remarkable increase of stress for oxygen deficient growth, as indicated by the green data points. We observe a monotonic positive stress change up to 6 uc followed by a constant stress level. The slope of the first part of the curve corresponds to a film stress of +3.5 GPa and an averaged value of +2.7 GPa is obtained based on the total film thickness of 8 uc.

In all stress measurements we observe slight undulations of the stress signal during the measurement, which are not related to the PLD growth. Rather, they are ascribed to small thermal drift related variations of the curvature signal.

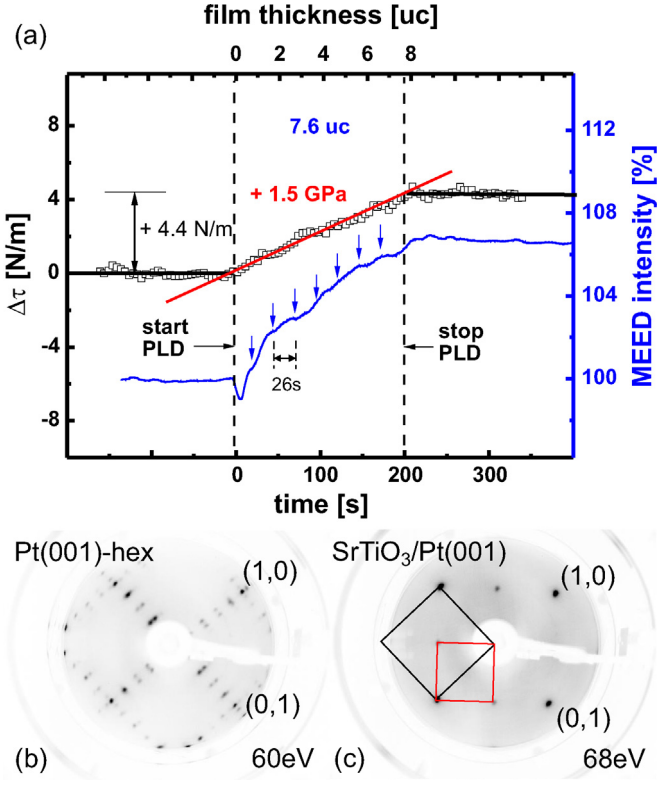

Fig. 2. Stress change $\Delta\tau$ (black squares) and MEED intensities (blue line) during PLD growth of $SrTiO_3$ on Pt(0 0 1). Vertical lines indicate when the PLD deposition started and stopped (T_{growth} = 900 K, $p_{O_2} = 1 \times 10^{-4}$ mbar). The LEED diffraction image below the stress measurement shows the clean substrate surfaces before PLD growth (b). Additional diffraction spots along [0,1] and [1,0] indicate the so-called hexagonal reconstruction of Pt(0 0 1) [42]. The diffraction pattern after growth (c) shows a c(2 × 2) superstructure (red square), where the 1 × 1 mesh is indicated in black. (For interpretation of the references to color in this figure legend, the reader is referred to the web version of the article.)

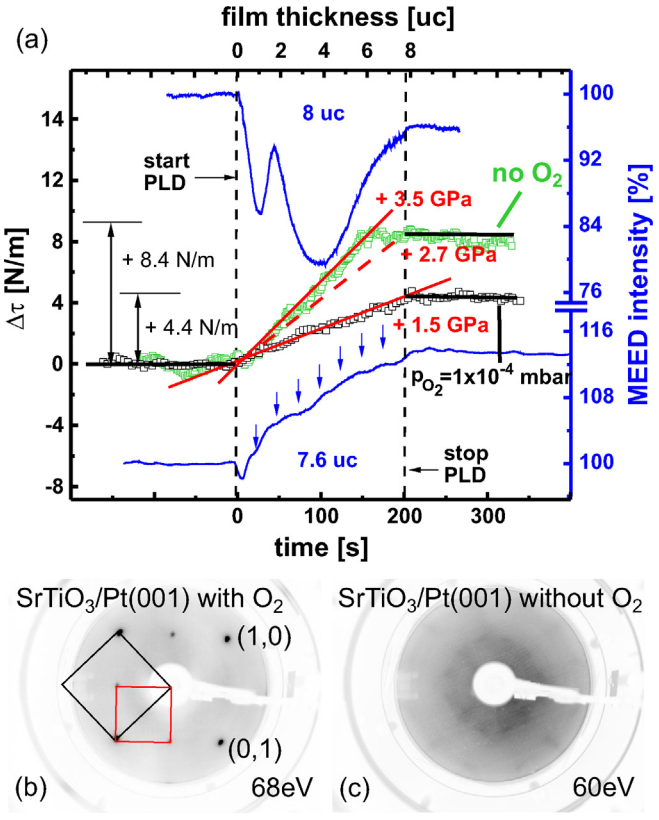

Fig. 3. Stress change $\Delta\tau$ during PLD growth of $SrTiO_3$ on Pt(0 0 1) under different oxygen partial pressures (T_{growth} = 940 K), black data points: $p_{O_2} = 1 \times 10^{-4}$ mbar, green data points: $p_{O_2} < 1 \times 10^{-10}$ mbar. Vertical lines indicate when the deposition started and stopped. The upper MEED intensity curve (blue line) is obtained during oxygen deficient growth, the lower one is measured during growth at $p_{O_2} = 1 \times 10^{-4}$ mbar. The LEED diffraction images show in (b) and (c) diffraction pattern of $SrTiO_3$ growth with and without additional O_2 pressure, respectively. The 1 × 1 Pt substrate unit cell is indicated by the black square, and the c(2 × 2) superstructure mesh is shown in red. No clear diffraction pattern is observed without O_2 in (c). (For interpretation of the references to color in this figure legend, the reader is referred to the web version of the article.)

4. Discussion

The quantitative analysis of film stress requires the knowledge of the specific film–substrate epitaxial orientation, as elasticity shows pronounced anisotropy. A hard spheres model of the atomic arrangement between film an substrate was presented in previous LEED, STM and XRD structural investigations [14,15,17]. Our LEED results are in agreement with this model, and we apply it here to analyze our data.

According to this structural model, the [1 0 0] direction of the epitaxial $BaTiO_3$ and $SrTiO_3$ films is aligned along the [1 0 0] direction of the fcc Pt substrate. The oxygen atoms of the film are located on top of the Pt atoms [14]. The main characteristic of the structural model is a cubic (0 0 1) film orientation, in agreement with the observed LEED patterns.

To appreciate the measured stress values we compare experimental film stress with the calculated stress, based on continuum bulk-like film elasticity and epitaxial misfit. To this end we define the epitaxial misfit as $\eta = (a_s - a_f)/a_f$. We assume a biaxial isotropic film strain which is given by this misfit. This induces a film stress of $\tau_{calc} = (Y/(1-\nu)) \cdot \eta$, where Y and ν are the Young modulus and the Poisson ratio of the film, respectively. An overview of the substrate and film elastic constants is given in Table 1. All elastic constants are given at room temperature. Literature values for the temperature dependence of the elastic constants are given for Pt [54], but not for cubic $BaTiO_3$. However, in view of the sizable error bars, we prefer to use room temperature values instead for both film and substrate. As temperature effects affect both substrate and film, we expect only a small correction of the calculated film stress of less than 10%.

Table 2 summarizes the experimental film stress τ_{exp}, the lattice misfit η and the calculated film stress τ_{calc}. Tabulated film and substrate bulk lattice spacings (a_f, a_s) and elastic compliance constants s_{ij} of the film material were used to calculate η and τ_{calc}. We find for both films a favorable agreement between calculated and measured film stress. We conclude that epitaxial misfit is the dominant origin of film stress in these examples. For these specific cases, interfacial stress and surface stress changes are negligible in view of misfit-induced stress [37,40].

Our stress curves show a constant slope during deposition. This indicates that all film material contributes identically to the stress change. This speaks in favor of pseudomorphic growth, where the film strain remains constant throughout the film thickness. Thus we deduce that the critical thickness for epitaxial growth on Pt(0 0 1) under our growth conditions is larger than 18 uc (7.2 nm) for $BaTiO_3$ and larger than 8 uc (3.1 nm) for $SrTiO_3$. Previous work reported film strain relaxations in $BaTiO_3$ for growth on $SrTiO_3$ starting around 5 nm film thickness [55]. In this former work $BaTiO_3$ was exposed to a larger misfit of −2.7% as compared to −2.3% for the growth on Pt(0 0 1) studied here, and the observation of a larger critical thickness here appears plausible. A detailed study of stress in thicker films and the study of the role of temperature for the resulting film stress are topics of future work.

The structural complexity of bulk $BaTiO_3$ gives rise to an important question regarding the proper reference state for the calculation of misfit. Bulk $BaTiO_3$ shows a phase transition [56] from a tetragonal to a cubic lattice structure with increasing temperature near 400 K. This raises the question which reference state should be used for a few atomic layer thin film grown at 870–1000 K under compressive strain of −2%? This is *a priori* not clear. The high growth temperature may speak in favor of a cubic lattice. However, theory predicts [18,57] a substantial increase of the transition temperature in strained films as compared to bulk. Thus, tetragonal $BaTiO_3$ might be the proper reference state for our growth even at 900 K.

The resulting misfit strain depends on the reference state. In the case of cubic $BaTiO_3$, an in-plane misfit of $\eta = (a_s - a_{ref})/a_{ref} = -2.3\%$ results. Reference to the tetragonal lattice leads to a smaller in-plane and a larger out-of-plane lattice constant ($a = b = 3.992$Å and $c = 4.036$Å) [58], which results in a smaller misfit of $\eta = -1.9\%$.

Our stress measurements open an independent approach to identify the proper reference state. The film stress, which is calculated for the cubic and the tetragonal case by $\tau = (Y/(1-\nu)) \cdot \eta$[1] amounts to −4.3 GPa and −3.2 GPa, respectively. The comparison with the experimental value of -4.2 ± 0.4 GPa leads to a very good quantitative agreement with the calculation for the cubic reference structure. This speaks in favor of a cubic lattice structure as the proper reference state.

Finally, we address the role of oxygen partial pressure during PLD for the resulting film stress. The application of an oxygen partial pressure during PLD growth of perovskite oxides is a common procedure to account for oxygen deficiencies which would otherwise result during PLD growth [59]. A detailed understanding of the underlying processes, which leads to the notion that an oxygen partial pressure ensures stoichiometric and epitaxial growth during PLD, is still under debate [50,60], and the applied growth procedures reflect the best outcome based on empirical findings.

The oxygen partial pressure during film growth influences both epitaxial order and stress substantially, as shown in Fig. 3. It is apparent, that in the oxygen deficient case no long range epitaxial order was obtained by LEED, although thickness and growth temperature were comparable to the growth conditions with O_2 partial pressure. Furthermore, a two times larger stress change of +8.4 N/m was found in the absence of an oxygen background pressure, as compared to +4.4 N/m with oxygen partial pressure.

How can we understand film stress in the absence of a LEED pattern? The stress measurement is sensitive to any local variation of forces acting in the film, and it averages over the whole crystal surface. The observation of a LEED pattern implies that on a larger lateral scale of order of the transfer width (10–100 nm), an ordered atomic arrangement is observed. Thus, the absence of a distinct LEED pattern indicates that no long range order is established. However, locally, on the atomic scale, still atomic bonds may be strained, giving rise to film stress. Further structural characterizations, also by *e.g.* HR-TEM would be helpful to characterize the film structure. However, corresponding studies have not been performed yet.

PLD growth with and without oxygen partial pressure, as presented in Fig. 3, leads to different film stress. The question arises to which extend a different film stoichiometry can be hold responsible for this. To offer some first qualitative insights we present Auger electron spectroscopy (AES) data in Fig. 4. We observe a slightly smaller oxygen intensity ratio for oxygen deficient growth as compared to growth under oxygen partial pressure. Interestingly, also the Ti/Sr AES intensity ratio differs slightly for both preparation conditions. A quantitative analysis of these findings and further stoichiometric characterization of the films would be beneficial, but this goes beyond the scope of this work. We conclude that the preparation conditions influence the stoichiometry of the film.

The observed increase of film stress upon oxygen partial pressure reduction is remarkable and contra-intuitive in view of previous work. In previous investigations it was reported that a reduced oxygen partial pressure increases the out-of-plane film lattice parameter for homoepitaxy of $SrTiO_3$ [48] and $SrTiO_3/BaTiO_3$ superlattices [49]. These results imply that oxygen deficiency leads to an enlarged lattice.

[1] The in-plane biaxial modulus for cubic and tetragonal $BaTiO_3$ is 187 GPa and 168 GPa, respectively. The corresponding misfit values are −2.3% for the cubic case and −1.9% for the tetragonal case under the assumption of c-domains perpendicular to the substrate surface.

Table 2
Overview of lattice misfit η and calculated film stress τ_{calc} based on room temperature bulk lattice constants and linear elasticity. The measured film stress τ_{exp} is given for comparison.

Substrate	Film	Film thickness (uc)	Lattice constant a (Å)	$\eta = \frac{a_S - a_f}{a_f}$ (%)	$\tau_{calc} = \frac{Y}{1-\nu} \cdot \eta$ (GPa)	τ_{exp} (GPa)
Pt(0 0 1)	$BaTiO_{3cub}$	18	4.012	−2.3	−4.3	-4.2 ± 0.4
a_{Pt}=3.920Å	$SrTiO_3$	7.5	3.905	+0.4	+1.4	$+1.5 \pm 0.2$

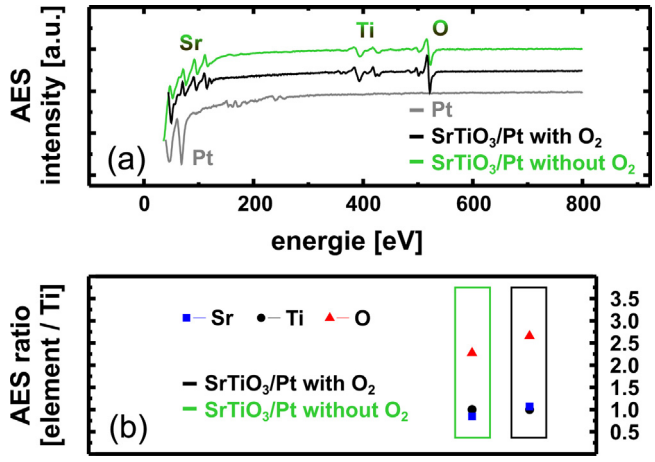

Fig. 4. (a) Auger electron spectra (AES) of the clean Pt substrate and after $SrTiO_3$ growth presented in Fig. 3. Green and black curves correspond to oxygen-deficient growth and to growth with an oxygen partial pressure, as outlined in Fig. 3. The spectra are shifted vertically for clarity. (b) AES intensity ratios of the elements Sr, Ti and O, normalized to Ti, are extracted from (a). The data are grouped within a rectangular box according to the preparation conditions, as outlined in Fig. 3. (For interpretation of the references to color in this figure legend, the reader is referred to the web version of the article.)

Thus, an increase of the in-plane lattice constant for oxygen deficient growth would be expected. This implies that the misfit for $SrTiO_3$ on Pt(0 0 1) would be reduced from its tensile value. This is at variance with our stress measurements presented in Fig. 3. If we tentatively ascribe the observed stress variation by a factor of two to a change of misfit, then an increase of the misfit from +0.4% to +0.8% should be considered to explain the stress result, in sharp contrast to the argument presented above.

This surprising result may indicate that in addition to lattice distortions upon oxygen partial pressure variations also other mechanisms need to be considered. One possible aspect is the change of the elastic properties of the film. In view of our example we may speculate that the biaxial modulus becomes stiffer upon oxygen deficiency. However these considerations appear to be a bit far-fetched in regard of the absence of long-range epitaxial order for oxygen deficient growth. Thus we cannot discriminate between oxygen-induced strain and elasticity variations.

In addition, the PLD process itself is expected to be susceptible to partial pressure effects. Any variation of the partial pressures will influence the moderating function of the gas phase, which might impact implantation effects in the growing film, caused by high energetic particles originating from the PLD plasma near the target [48]. At present, we cannot offer any insights into the respective stress variation.

Although we are not able to provide a definite explanation for the impact of oxygen partial pressure on film stress in PLD growth yet, our results show the crucial role of oxygen for modification of the film structure indicating the high complexity of these systems. A comparison between experimental observations, where experimental parameters, including oxygen partial pressure are not identical, appears questionable.

5. Conclusions

This work provides quantitative data on film stress in $BaTiO_3$ and $SrTiO_3$ films, which may serve as reference for future theoretical investigations. We find film stress of the order of GPa, which can be quantitatively described by misfit strain, using continuum elasticity. The quantitative analysis of stress identifies cubic $BaTiO_3$/Pt(0 0 1) as the proper reference state. Oxygen partial pressure was identified to play a very important role for the resulting film stress. A thorough understanding of the relation between stress and strain and preparation conditions is still at its infancy and further experimental and theoretical investigations are called for.

Acknowledgment

Partial financial support by DFG SFB 762 is gratefully acknowledged.

References

[1] Y. Maeno, H. Hashimoto, K. Yoshida, S. Nishizaki, T. Fujita, J. Bednorzt, F. Lichtenberg, Superconductivity in a layered perovskite without copper, Nature 372 (6506) (1994) 532–534.
[2] I. Grinberg, D.V. West, M. Torres, G. Gou, D.M. Stein, L. Wu, G. Chen, E.M. Gallo, A.R. Akbashev, P.K. Davies, J.E. Spanier, A.M. Rappe, Perovskite oxides for visible-light-absorbing ferroelectric and photovoltaic materials, Nature 503 (7477) (2013) 509–512.
[3] K. Abe, N. Yanase, K. Sano, M. Izuha, N. Fukushima, T. Kawakubo, Modification of ferroelectricity in heteroepitaxial (Ba, Sr)TiO_3 films for non-volatile memory applications, Integr. Ferroelectr. 21 (1–4) (1998) 197–206.
[4] L. Martin, Y.-H. Chu, R. Ramesh, Advances in the growth and characterization of magnetic, ferroelectric, and multiferroic oxide thin films, Mater. Sci. Eng. R: Rep. 68 (4–6) (2010) 89–133.
[5] M. Bibes, J.E. Villegas, A. Barthelemy, Ultrathin oxide films and interfaces for electronics and spintronics, Adv. Phys. 60 (1) (2011) 5–84.
[6] S.A. Wolf, D.D. Awschalom, R.A. Buhrman, J.M. Daughton, S. von Molnár, M.L. Roukes, A.Y. Chtchelkanova, D.M. Treger, Spintronics: a spin-based electronics vision for the future, Science 294 (5546) (2001) 1488–1495.
[7] N.A. Spaldin, M. Fiebig, The renaissance of magnetoelectric multiferroics, Science 309 (5733) (2005) 391–392.
[8] H.D. Megaw, Crystal structure of barium titanate, Nature 155 (1945) 484.
[9] H.D. Megaw, Crystal structure of double oxides of the perovskite type, Proc. Phys. Soc. 58 (2) (1946) 133.
[10] J.K. Hulm, The dielectric properties of some alkaline earth titanates at low temperatures, Proc. Phys. Soc. A 63 (10) (1950) 1184.
[11] G.M. Davis, M.C. Gower, Epitaxial growth of thin films of $BaTiO_3$ using excimer laser ablation, Appl. Phys. Lett. 55 (2) (1989) 112–114.
[12] J. Gong, M. Kawasaki, K. Fujito, U. Tanaka, N. Ishizawa, M. Yoshimoto, H. Koinuma, M. Kumagai, K. Hirai, K. Horiguchi, Heteroepitaxial growth of c-axis-oriented $BaTiO_3$ thin films with an atomically smooth surface, Jpn. J. Appl. Phys. 32 (Part 2, No. 5A) (1993) L687–L689.
[13] T. Nakamura, H. Inada, M. Iiyama, In situ surface characterization of $SrTiO_3$(1 0 0) substrates and homoepitaxial $SrTiO_3$ thin films grown by molecular beam epitaxy and pulsed laser deposition, Appl. Surf. Sci. 130–132 (1998) 576–581.
[14] H.L. Meyerheim, F. Klimenta, A. Ernst, K. Mohseni, S. Ostanin, M. Fechner, S. Parihar, I.V. Maznichenko, I. Mertig, J. Kirschner, Structural secrets of multiferroic interfaces, Phys. Rev. Lett. 106 (8) (2011) 087203.
[15] H.L. Meyerheim, A. Ernst, K. Mohseni, I.V. Maznichenko, J. Henk, S. Ostanin, N. Jedrecy, F. Klimenta, J. Zegenhagen, C. Schlueter, I. Mertig, J. Kirschner, Tuning the structure of ultrathin $BaTiO_3$ films on Me(0 0 1) (Me = Fe, Pd, Pt) surfaces, Phys. Rev. Lett. 111 (10) (2013) 105501.
[16] S. Foerster, W. Widdra, Growth, structure, and thermal stability of epitaxial $BaTiO_3$ films on Pt(1 1 1), Surf. Sci. 604 (23–24) (2010) 2163–2169.
[17] S. Foerster, M. Huth, K.-M. Schindler, W. Widdra, Epitaxial $BaTiO_3$ (1 0 0) films on Pt(1 0 0): a low-energy electron diffraction, scanning tunneling microscopy, and X-ray photoelectron spectroscopy study, J. Chem. Phys. 135 (10) (2011) 104701-1–104701-6.
[18] Y.L. Li, L.Q. Chen, Temperature-strain phase diagram for $BaTiO_3$ thin films, Appl. Phys. Lett. 88 (7) (2006) 072905-1–072905-3.

[19] M. Fechner, I.V. Maznichenko, S. Ostanin, A. Ernst, J. Henk, P. Bruno, I. Mertig, Magnetic phase transition in two-phase multiferroics predicted from first principles, Phys. Rev. B 78 (21) (2008) 212406.
[20] U. Aschauer, R. Pfenninger, S.M. Selbach, T. Grande, N.A. Spaldin, Strain-controlled oxygen vacancy formation and ordering in $CaMnO_3$, Phys. Rev. B 88 (5) (2013) 054111.
[21] W. Eerenstein, N.D. Mathur, J.F. Scott, Multiferroic and magnetoelectric materials, Nature 442 (7104) (2006) 759–765.
[22] F. Spaepen, Interfaces and stresses in thin films, Acta Mater. 48 (1) (2000) 31–42.
[23] F. Spaepen, A.L. Shull, Mechanical properties of thin films and multilayers, Curr. Opin. Solid State Mater. Sci. 1 (5) (1996) 679–683.
[24] R. Koch, M. Weber, K. Thürmer, K. Rieder, Magnetoelastic coupling of Fe at high stress investigated by means of epitaxial Fe(0 0 1) films, J. Magn. Magn. Mater. 159 (1–2) (1996) L11–L16.
[25] D. Sander, The correlation between mechanical stress and magnetic anisotropy in ultrathin films, Rep. Prog. Phys. 62 (5) (1999) 809.
[26] D. Sander, S. Ouazi, V.S. Stepanyuk, D.I. Bazhanov, J. Kirschner, Stress oscillations in a growing metal film, Surf. Sci. 512 (3) (2002) 281–286.
[27] W. Pan, D. Sander, M.-T. Lin, J. Kirschner, Stress oscillations and surface alloy formation during the growth of FeMn on Cu(0 0 1), Phys. Rev. B 68 (22) (2003) 224419.
[28] R. Koch, Stress in evaporated and sputtered thin films – a comparison, Surf. Coat. Technol. 204 (12–13) (2010) 1973–1982.
[29] H. Krebs, Characteristic properties of laser-deposited metallic systems, Int. J. Non-Equilib. Process. 10 (1997) 3–24.
[30] T. Scharf, J. Faupel, K. Sturm, H.-U. Krebs, Intrinsic stress evolution in laser deposited thin films, J. Appl. Phys. 94 (7) (2003) 4273–4278.
[31] S. Roy, H.L. Meyerheim, K. Mohseni, Z. Tian, D. Sander, M. Hoffmann, W. Adeagbo, A. Ernst, W. Hergert, R. Felici, J. Kirschner, X-ray analysis of wurtzite-type CoO(1 1 1) films on Ir(0 0 1): correlation of structure, stress, electronic, and magnetic properties, Phys. Rev. B 89 (2014) 165428.
[32] D. Sander, S. Ouazi, A. Enders, T. Gutjahr-Löser, V.S. Stepanyuk, D.I. Bazhanov, J. Kirschner, Stress, strain and magnetostriction in epitaxial films, J. Phys.: Condens. Matter 14 (16) (2002) 4165.
[33] A.G. Every, A.K. McCurdy, Elastic Constants s, c – Cubic System. Elements (Landolt Börnstein – Numerical Data and Functional Relationships in Science and Technology, Group III), vol. 29a, Springer, Berlin, Heidelberg, 1992.
[34] A.G. Every, A.K. McCurdy, Elastic Constants s, c – Cubic System. Miscell. Comp. (Landolt Börnstein – Numerical Data and Functional Relationships in Science and Technology, Group III), vol. 29a, Springer, Berlin, Heidelberg, 1992.
[35] A.G. Every, A.K. McCurdy, Elastic Constants s, c – Tetragonal System, 6 Constants (Landolt Börnstein – Numerical Data and Functional Relationships in Science and Technology, Group III), vol. 29a, Springer, Berlin, Heidelberg, 1992.
[36] T. Gutjahr-Löser, Magnetoelastische Kopplung in oligatomaren Filmen, Martin-Luther-Universität Halle-Wittenberg, 1999 (Ph.D. thesis).
[37] D. Sander, Surface stress: implications and measurements, Curr. Opin. Solid State Mater. Sci. 7 (1) (2003) 51–57.
[38] J. Premper, D. Sander, J. Kirschner, A combined surface stress and magneto-optical Kerr effect measurement setup for temperatures down to 30 K and in fields of up to 0.7 T, Rev. Sci. Instrum. 83 (7) (2012) 073904–073908.
[39] MaTeck GmbH, Im Langenbroich 20, D-52428 Jülich, http://www.mateck.de
[40] H. Ibach, The role of surface stress in reconstruction, epitaxial growth and stabilization of mesoscopic structures, Surf. Sci. Rep. 29 (5–6) (1997) 195–263.
[41] K. Dahmen, S. Lehwald, H. Ibach, Bending of crystalline plates under the influence of surface stress – a finite element analysis, Surf. Sci. 446 (1–2) (2000) 161–173.
[42] P. Heilmann, K. Heinz, K. Mueller, The superstructures of the clean Pt(1 0 0) and Ir(1 0 0) surfaces, Surf. Sci. 83 (2) (1979) 487–497.
[43] $BaTiO_3$, 99.9 %, ø, 25 mm × 3 mm; MaTeck GmbH, Im Langenbroich 20, D-52428 Jülich, http://www.mateck.de
[44] $SrTiO_3$, 99.9 %, ø 25mm × 3 mm; MaTeck GmbH, Im Langenbroich 20, D-52428 Jülich, http://www.mateck.de
[45] Coherent Lambda Physik GmbH, Hans-Böckler-Strasse 12, D-37079 Göttingen, Germany, http://www.coherent.com
[46] XTC/2 Deposition Controller, LEYBOLD INFICON INC., Two Technology Place East Syracuse, New York, December 1993 http://www.inficon.com
[47] J.B. Goodenough, M. Longo, Table 2, Part 1 in 3.1.7 Data: Crystallographic Properties of Compounds with Perovskite or Perovskite-Related Structure (Landolt Boernstein – Numerical Data and Functional Relationships in Science and Technology, Group III), Vol. 4a: Magnetic and Other Properties of Oxides and Related Compounds, Part A, SpringerMaterials – The Landolt–Börnstein Database, Springer, Berlin, Heidelberg, 1970.
[48] E.J. Tarsa, E.A. Hachfeld, F.T. Quinlan, J.S. Speck, M. Eddy, Growth-related stress and surface morphology in homoepitaxial $SrTiO_3$ films, Appl. Phys. Lett. 68 (4) (1996) 490–492.
[49] B.R. Kim, T.-U. Kim, W.-J. Lee, J.H. Moon, B.-T. Lee, H.S. Kim, J.H. Kim, Effects of periodicity and oxygen partial pressure on the crystallinity and dielectric property of artificial $SrTiO_3/BaTiO_3$ superlattices integrated on Si substrates by pulsed laser deposition method, Thin Solid Films 515 (16) (2007) 6438–6441.
[50] A. Khodan, S. Guyard, J.-P. Contour, D.-G. Crété, E. Jacquet, K. Bouzehouane, Pulsed laser deposition of epitaxial $SrTiO_3$ films: growth, structure and functional properties, Thin Solid Films 515 (16) (2007) 6422–6432.
[51] W. Brantley, Calculated elastic constants for stress problems associated with semiconductor devices, J. Appl. Phys. 44 (1) (1973) 534–535.
[52] D. Sander, Z. Tian, J. Kirschner, Cantilever measurements of surface stress, surface reconstruction, film stress and magnetoelastic stress of monolayers, Sensors 8 (7) (2008) 4466–4486.
[53] J. Premper, Mechanische Spannungen von $BaTiO_3$ und $SrTiO_3$ Atomlagen auf Metalleinkristallen, Martin-Luther-Universität Halle-Wittenberg, 2014 (Ph.D. thesis).
[54] A.G. Every, A.K. McCurdy, Temperature Coefficients Tc – Table 28. Cubic System. Elements. (Landolt Börnstein – Numerical Data and Functional Relationships in Science and Technology, Group III), Vol. 29a, SpringerMaterials – The Landolt–Börnstein Database, Springer, Berlin, Heidelberg, 1992.
[55] A. Visinoiu, M. Alexe, H.N. Lee, D.N. Zakharov, A. Pignolet, D. Hesse, U. Gösele, Initial growth stages of epitaxial $BaTiO_3$ films on vicinal $SrTiO_3$ (0 0 1) substrate surfaces, J. Appl. Phys. 91 (12) (2002) 10157–10162.
[56] L.A. Shebanov, X-ray temperature study of crystallographic characteristics of barium titanate, Phys. Solidi (a) 65 (1) (1981) 321–325.
[57] K.J. Choi, M. Biegalski, Y.L. Li, A. Sharan, J. Schubert, R. Uecker, P. Reiche, Y.B. Chen, X.Q. Pan, V. Gopalan, L.-Q. Chen, D.G. Schlom, C.B. Eom, Enhancement of ferroelectricity in strained $BaTiO_3$ thin films, Science 306 (5698) (2004) 1005–1009.
[58] M. Adachi, Y. Akishige, T. Asahi, K. Deguchi, K. Gesi, K. Hasebe, T. Hikita, T. Ikeda, Y. Iwata, M. Komukae, T. Mitsui, E. Nakamura, N. Nakatani, M. Okuyama, T. Osaka, A. Sakai, E. Sawaguchi, Y. Shiozaki, T. Takenaka, K. Toyoda, T. Tsukamoto, T. Yagi, $BaTiO_3$ (Cubic) [F] Survey, 1A-10. (Landolt Boernstein – Numerical Data and Functional Relationships in Science and Technology, Group III), Vol. 36A1: Oxides, SpringerMaterials – The Landolt–Börnstein Database, Springer, Berlin, Heidelberg, 2001.
[59] P. Willmott, Deposition of complex multielemental thin films, Prog. Surf. Sci. 76 (6–8) (2004) 163–217.
[60] J. Gonzalo, C.N. Afonso, J. Perriere, The role of film re-emission and gas scattering processes on the stoichiometry of laser deposited films, Appl. Phys. Lett. 67 (9) (1995) 1325–1327.